An International Journal of Optimization and Control: Theories & Applications
ISSN: 2146-0957 eISSN: 2146-5703
Vol.X, No.X, pp.X-X (2026)
https://doi.org/10.36922/IJOCTA026260133

RESEARCH ARTICLE

Optimization of pontoon and rotating-frame parameters during launching and transportation of offshore platform support blocks

Latif F. Aslanov[1,2†*], Ulvi L. Aslanli[3,4†], and Firidun L. Aslanov[2,5]

[1]Department of Diagnostics of Oil and Gas Production Facilities, Oil Gas Scientific Research Project Institute, State Oil Company of the Republic of Azerbaijan, Baku, Azerbaijan

[2]Department of Land Reclamation and Water Management Construction, Azerbaijan University of Architecture and Construction, Baku, Azerbaijan

[3]Department of Foundations and Underground Structures, Faculty of Construction, Azerbaijan University of Architecture and Construction, Baku, Azerbaijan

[4]SOCAR Downstream Management, Baku, Azerbaijan

[5]SOCAR STAR Refinery, İzmir, Türkiye

latif.aslanov@bk.ru; ulviaslanli898@gmail.com; firidun-aslanov@mail.ru

ARTICLE INFO

Article history:
Received: June 25, 2026
Revised: July 29, 2026
Accepted: August 10, 2026
Published Online: November 20, 2026

Keywords:
Pontoon structures
Physical material properties
Stress–strain state
Nonlinear model
Support block

AMS Classification 2010:
90B23, 90B56

ABSTRACT

Offshore pontoon structures and rotating-frame launching systems are subjected to complex loading conditions, necessitating accurate assessment of their nonlinear structural behavior and the load-carrying capacity of critical components to ensure safe and reliable operations. This study presents a nonlinear computational framework for analyzing the stress–strain behavior of offshore pontoon structures subjected to combined internal and external loading conditions. The objective is to improve the accuracy of structural assessment by considering both material nonlinearity and geometric variability and to evaluate the performance of rotating-frame rollers used during offshore support-block launching operations. The structural response is described using the momentless theory of shells of revolution combined with a physically nonlinear constitutive model. The governing equations are solved using the small parameter method and a finite-difference numerical scheme. In addition, experimental investigations were performed on hollow and composite-filled rotating-frame rollers to assess their load-carrying performance under transverse static loading. The proposed nonlinear formulation predicts a reduction of 21.9% in the calculated maximum stress compared with the classical linear model, while geometric optimization results in an additional 7.5% reduction. Experimental results demonstrate that filling the rollers with composite material increases their maximum load-carrying capacity by approximately 2.3 times compared with hollow rollers. The developed computational and experimental approach provides a reliable framework for the analysis, optimization, and design assessment of offshore pontoon structures and launching systems by integrating nonlinear shell modeling with experimental validation of critical load-bearing components.

CC BY

1. Introduction

The present study addresses the structural behavior of offshore pontoon structures and rotating-frame systems used during the launching and transportation of support blocks. Unlike conventional approaches focusing primarily on the strength assessment of floating structures,

†*These authors contributed equally to this work.*
*Corresponding Author

this study considers the combined effects of material nonlinearity, geometric parameters, and load redistribution in the pontoon structure, together with the load-carrying performance of the rotating-frame rollers.

A nonlinear analytical framework based on the momentless theory of shells of revolution and the small parameter method is developed to evaluate the stress–strain state of pontoon structures under combined internal and external loading conditions. The formulation accounts for physically nonlinear material behavior and enables the assessment of stress redistribution resulting from variations in structural parameters. The numerical solution is obtained using a finite-difference approach.

In addition, experimental investigations are conducted to evaluate the load-carrying capacity of hollow and composite-filled rollers used in the rotating-frame system. The combined computational and experimental approach provides an engineering basis for assessing pontoon structures and their supporting mechanisms, as well as for improving the structural performance and reliability of offshore support-block launching operations.

2. Literature review

2.1. Offshore structures and pontoon systems

The structural behavior of offshore platforms under blast loading,[1] the main types of fixed and floating offshore structures and their engineering applications,[2] probabilistic models for assessing the risks of accidents caused by ship–platform collisions,[3] opportunities for the reuse of offshore oil and gas platforms and the extension of their service life,[4] methods for reducing liquid sloshing in steel tanks,[5] the effectiveness of shock-absorbing systems designed to mitigate impacts during boat landings on fixed offshore platforms,[6] and the vibrations of partially submerged reservoirs and cylindrical supports under fluid–structure interaction conditions[7] have been investigated in the relevant studies.

The seismic behavior of elevated water tanks with innovative structural configurations,8 the seismic response of slender storage tanks with different support configurations,[9] the seismic response of topside equipment on fixed offshore platforms,[10] structural changes in multifaceted gas pipelines,[11] variations in the energy characteristics of pipeline systems under hydrodynamic loading,[12] the strength of liquid-filled tanks subjected to impact during free fall,[13] and the assessment of the lifecycle structural integrity of single point anchor reservoir offshore platforms using a composite degradation index[14] have been investigated in the relevant studies.

2.2. Nonlinear analysis and numerical modeling of shell structures

Geometric nonlinearity in the finite element analysis of reinforced concrete columns,[15] the elastic–plastic behavior of pipes and vertical risers in offshore hydraulic structures,[16] the buckling behavior of dented cylindrical shells reinforced with carbon fiber-reinforced polymer,[17] the mathematical analysis of the mathematical analysis of a nine-node mixed-interpolation shell element for plate-bending problems,[18] mathematical and computational methods for solving problems using Wolfram Mathematica software,[19] and the seismic performance and fragility of unanchored cylindrical steel tanks under earthquake loading[20] have been investigated in previous studies. The fundamental principles of finite element analysis of shell structures,[21] the influence of local geometric imperfections on the dynamic buckling behavior of cylindrical storage tanks,[22] and the formulation of finite deformation in thin shells using the analytical mechanics of material surfaces[23] have also been examined.

Further studies have addressed the stress–strain behavior and load-bearing capacity of compressed concrete-filled pipe elements,[24] the development of an interface finite element for modeling localized membrane and bending deformations in shell structures,[25] the nonlinear vibration behavior of partially filled multilayer cylindrical tanks considering fluid–structure interaction and sloshing effects,[26] the buckling behavior of imperfect cylindrical shells under axial loading using gene expression programming,[27] the buckling behavior of steel tanks with horizontal geometric imperfections,[28] and the influence of localized defects on the buckling behavior of cylindrical shells under axial compression.[29]. In addition, the influence of annular plate dimensions on the stress–strain behavior of steel tanks,[30] nonlinear terms in large-deformation models of thin-walled cylindrical shells,[31] and comparisons between software-based modeling results and Eurocode calculations for liquid-storage tank design[32] have been investigated.

Other studies have focused on the semi-analytical modeling of buckling and stress behavior in pressurized composite cylinders,[33] the

assessment of the stress–strain state of vertical steel tanks using laser-scanning data,[34] the geometrically nonlinear behavior of laminated shells using an isogeometric finite element formulation,[35] the nonlinear dynamic response and damage characteristics of small-scale all-concrete liquefied natural gas storage tanks subjected to penetration and explosion loadings through numerical modeling,[36] the identification of structural shape features and the updating of finite element models using full-field strain data,[37] the buckling behavior of cylindrical shells with an axially varying elastic modulus under external pressure,[38] the finite element assessment of the buckling capacity of conical steel tanks incorporating field-measured initial geometric imperfections,[39] and the numerical analysis of shells of revolution with arbitrary meridional variations.[40]

2.3. Research gap and study objectives

Although the mentioned approaches have significantly improved the prediction of structural behavior, relatively limited attention has been paid to the combined consideration of physically nonlinear shell formulations and the practical launching systems used for offshore support-block transportation. Therefore, the present study integrates a nonlinear shell model based on the small parameter method with an experimental investigation of rotating-frame rollers, providing a unified computational and experimental framework for the analysis of offshore pontoon launching systems.

3. Problem description and engineering background

The structural integrity of offshore support blocks during launching and transportation is a critical aspect of marine engineering design. Accurate assessment of loads, buoyancy effects, and stress–strain behavior is essential for ensuring the safety and reliability of these large-scale structures throughout all operational stages.

The support block is fabricated and assembled at the slipway of the Baku Deepwater Jackets Plant named after Heydar Aliyev. The arrangement of the support block on the slipway is shown in **Figure 1**. The slipway consists of two parallel beams, serving as the primary structural foundation for assembly and launching operations. The launching system consists of a coastal concrete foundation equipped with a steel sliding platform, providing a continuous surface for the movement of the structure. To reduce friction during the movement of the support block along the slipway, the sliding tracks are coated with Teflon. This low-friction material ensures that the coefficient of friction remains within operationally acceptable limits, thereby facilitating safe and efficient transfer of the structure during the launching process.

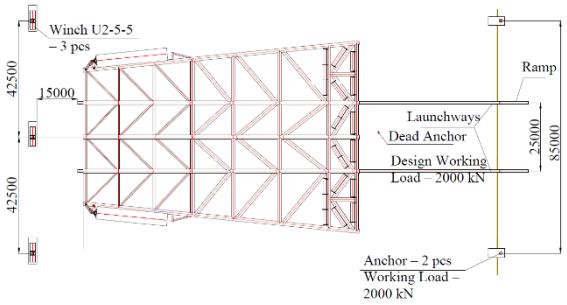


Figure 1. Arrangement of support block on the slipway

During the launching operation, the support block is moved by a push-pull system linked to the structure through an extension element and intermediate connection units. The applied load is transferred to the slipway beams and the rotating frame, while wooden runners installed beneath the central panel legs provide the required contact and support conditions. The required pulling force is evaluated analytically to verify the safe and reliable operation of the launching system.

For advancing the support block along the launching tracks and lowering it into the sea, a system of launch winches, anchored on standard concrete bases, is employed. Two lateral winches facilitate the forward movement, while a central winch serves both as a propulsion unit and a braking mechanism. A general view of the slipway of the Baku Deepwater Structures Factory is presented in **Figure 2**.

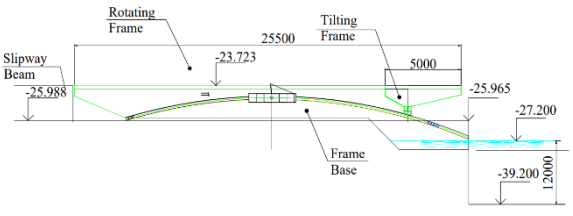


Figure 2. Slipway of the Baku Deepwater Structures Factory

Since the natural buoyancy of the support block is insufficient for the required operation,

supplementary flotation elements are introduced to provide safe movement during launching and transportation. The main pontoons are attached to the forward panels of the support block, while additional pontoons are positioned below the lower panel. Their geometric parameters and installation locations are determined through engineering analysis to maintain the necessary stability and flotation capacity during the launching process. The displacement of the support block during launching and pontoon dewatering is illustrated in **Figure 3**.

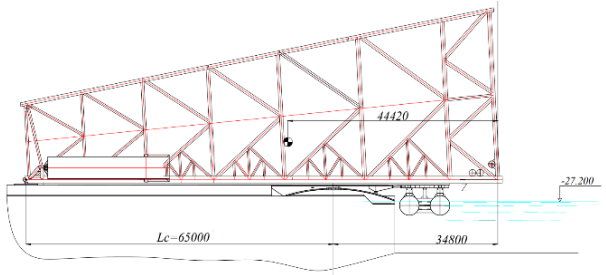


Figure 3. Displacement of the support block (Lc = 65.0 m). Pontoon dewatering. Lc is the distance between the capstan center and the frame axis.

The permissible load per unit length of the launching track depends on the geometry of the support block, the parameters of the launching system, and the mechanical characteristics of the sliding path. The limiting load distribution is determined by considering two governing factors: the force transfer between the forward and aft skids and the change in load intensity along the bow skid length.

The influence of the rotating-mechanism skid on the load distribution along the launching track is additionally investigated. The structural assessment includes the determination of longitudinal and transverse bending moments in the support block caused by gravitational loading and buoyancy effects. The calculations are performed for calm-water conditions with the support block considered at its transportation draft.

During towing, supplementary hydrodynamic effects associated with waves and currents are evaluated considering the selected towing speed and the environmental conditions expected along the transportation path. The stresses generated by these external actions are combined with the internal stresses caused by the overall bending response of the structure in still water, providing an integrated evaluation of the support block performance.

Following ballasting, the support block was rotated into a vertical position using a lifting system with a rated capacity of 4 MN (**Figures 4** and **5**). These operations were intended to maintain structural stability, control the center of gravity, and reduce the risk of overturning during lifting and positioning.

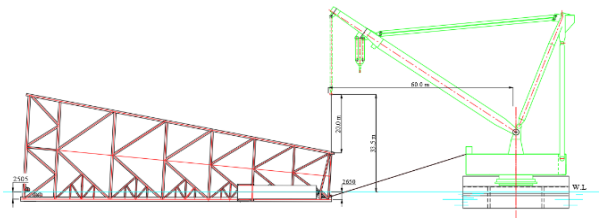


Figure 4. Hook slinging of the support block

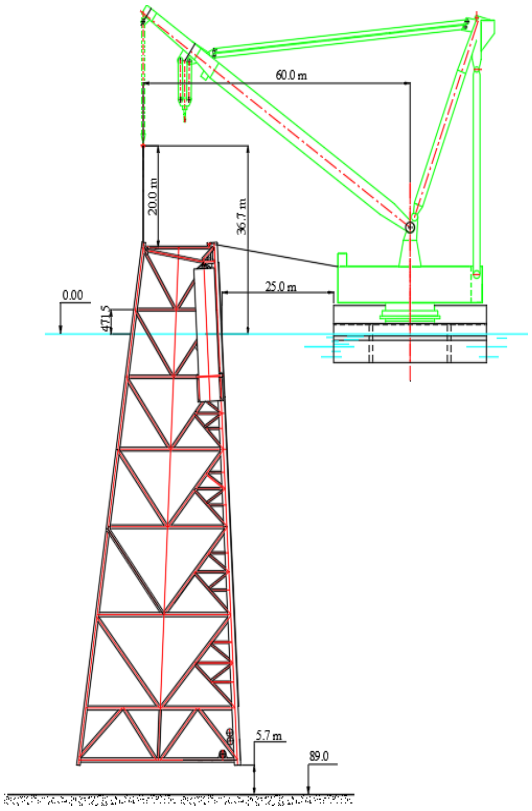


Figure 5. Ballasting of the support block and its rotation into a vertical position

The seating of the support block on the ground and its slinging using a hook is one of the important technological operations applied during the lifting and transportation of heavy loads. This process ensures the stable positioning of the equipment in its working state and guarantees the safe execution of lifting operations. The fastening and slinging mechanisms used in the support block system are capable of reliable performance

even under high-load conditions. A general view of this process is illustrated in **Figure 6**.

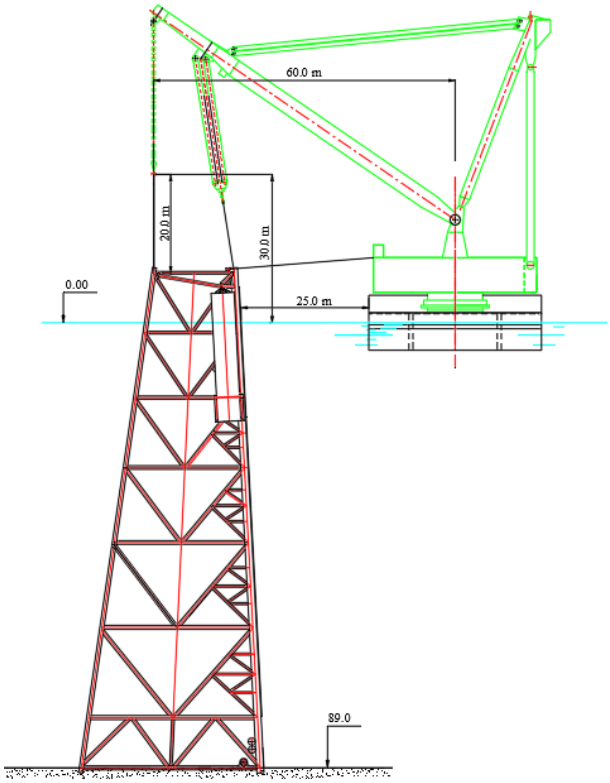


Figure 6. Ground seating and sling operation of the support block

4. Materials and methods

4.1. Structural model and assumptions

The offshore pontoon is modeled as a thin-walled shell of revolution subjected to combined internal and external loading. The structural response is described using the momentless (membrane) theory of shells, in which the load-carrying mechanism is governed solely by membrane forces, while bending moments and transverse shear forces are neglected. This assumption is appropriate for thin shells operating primarily under membrane action.

The shell is assumed to be homogeneous and isotropic, with constant thickness throughout the analyzed domain. The deformations are considered continuous and sufficiently smooth to satisfy the kinematic requirements of the membrane shell formulation. Material behavior is described by a physically nonlinear constitutive law, while the shell geometry is represented by the exact middle-surface geometry of the shell of revolution.

The structure is subjected to combined loading conditions representative of offshore launching and transportation operations, including internal pressure, external hydrostatic pressure, gravitational loading, and buoyancy effects. Both symmetric and asymmetric loading cases are considered to evaluate the stress–strain response under realistic operational conditions.

Figure 7 illustrates the initial configuration of the support block on the slipway and the rotating-frame launching system considered in the present study. This configuration forms the basis of the mathematical model and loading assumptions used throughout the analysis.

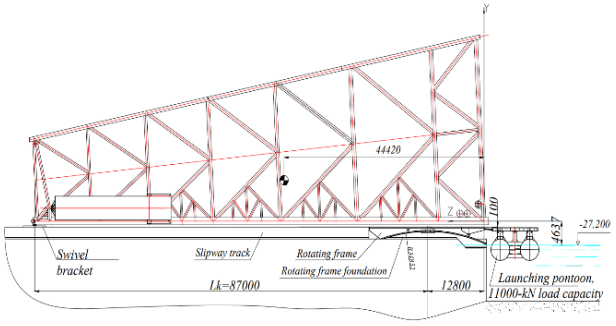


Figure 7. Initial configuration of the offshore support block, rotating frame, and slipway launching system used in the structural model (Lc = 87 m)

4.2. Governing equations

The fundamental equations governing the momentless shell theory, which are used to evaluate the structural strength and operational response of the pontoon structure, are expressed as follows.

$$\begin{aligned} &\frac{T_m}{R_m}+\frac{T_t}{R_t}=P_1 \quad ; \\ &\frac{1}{r}\frac{\partial}{\partial s}\left(T_m r\ sin\ \theta\right)-\frac{1}{r}\frac{\partial S}{\partial \varphi}sin\,\theta=P_2 \quad ; \\ &\frac{1}{r^2}\frac{\partial}{\partial s}\left(Sr^2\right)+\frac{1}{r}\frac{\partial T_t}{\partial \varphi}=-P_3 \quad , \end{aligned} \tag{1}$$

In **Equation 1**, T_m represents the meridional membrane force resultant, T_t denotes the circumferential membrane force resultant, and S represents the membrane shear force resultant. The terms P_1, P_2, and P_3 denote the meridional and tangential components of the applied planar forces, which act perpendicular to the shell surface. The radii of curvature in the meridional and tangential directions are represented by R_m

and R_t, respectively. The variables *r, q, j* and *s* correspond to the current spatial coordinates and geometric parameters.

$$\varepsilon_m = \frac{\partial u}{\partial s} + \frac{w}{R_m}; \varepsilon_t = \frac{\partial v}{r\partial \varphi} + \frac{v cos\ \theta}{r} + \frac{v}{R_t};$$
$$\gamma_{tm} = \frac{1}{r}\frac{\partial u}{d\varphi} + \frac{\partial v}{\partial s} - \frac{v}{r} cos\ \theta, \quad (2)$$

In **Equation 2**, ε_m and ε_t denote normal strains in the meridional and circumferential directions, respectively, while γ_{tm} represents the shear strain.

The complete list of symbols, definitions, units, and terminology used in the governing equations and mathematical formulation is provided in Appendix A (Table A1).

4.3. Nonlinear constitutive model

Taking the dependence between stress and strain as $\sigma = \varepsilon E - \beta\varepsilon^3$, we accept the physical equations as follows:[41]

$$E\varepsilon_m - \beta\varepsilon_m^3 = \frac{T_m - \mu T_t}{h}$$
$$E\varepsilon_t - \beta\varepsilon_t^3 = \frac{T_t - \mu T_m}{h} \quad (3)$$
$$G\gamma_{tm} - \beta_0\gamma_{tm}^3 = \frac{S}{h}$$

In **Equation 3**, E denotes the Young's modulus of the material, G represents the shear modulus, μ is Poisson's ratio, while β and β_0 are nonlinear material coefficients describing the deviation of the stress–strain relationship from linear elasticity in normal and shear deformation modes, respectively. The parameter h represents the shell thickness.

To analyze the stress–strain state of the pontoon under arbitrary external loading, taking into account the physical nonlinearity of the material, it is necessary to solve the nonlinear differential **Equations 1** and **3**. The small parameter method is employed to handle this complex problem, where the small parameter is introduced as described in:[42]

$$\nu = \frac{\beta\varepsilon_0^2}{E} = \frac{\beta_0\gamma_0^2}{G}, \quad (4)$$

The quantities ε_0 and γ_0 denote the characteristic normal and shear strain values corresponding to the material strength limit. This formula clearly illustrates that assuming the material is incompressible ($\mu = \frac{1}{2}$) leads to a specific simplification in the analysis.

$$\beta_0 = \frac{\beta\varepsilon_0^2}{3\gamma_0^2}, \quad (5)$$

We seek the solution of **Equations 1–3** by expanding the unknowns in a power series with respect to the small parameter *v*.

The formulation is developed in a generalized (dimensionless) form; therefore, no specific engineering material is prescribed. The material behavior is characterized by the elastic constants and nonlinear parameters appearing in the constitutive equations.

4.4. Small parameter method

The solution of **Equations 1–3** is obtained using the small parameter method. The unknown displacement components are expanded as power series with respect to the small parameter ν:

$$u = \sum_{j=0} u_j \cdot \nu^j;\ \nu = \sum_{j=0} \nu_j \cdot \nu^j;$$
$$w = \sum_{j=0} w_j \cdot \nu^j, \quad (6)$$

where u, ν, and w represent the meridional, circumferential, and normal displacement components of the shell middle surface, respectively, and ν is the small parameter defined in **Equation 4**.

Substituting **Equation 2** into **Equation 3** and considering the expansion given by **Equation 6**, the coefficients of identical powers of ν^j (j=0,1, 2...) are equated. This procedure leads to the following recurrent system of linear differential equations:

$$\frac{\partial u_0}{\partial s} + \frac{w_0}{R_m} = N_{1\kappa}(\varphi)$$
$$\frac{1}{r}\cdot\frac{\partial v_0}{\partial \varphi} + \frac{u_0}{r} cos\ \theta + \frac{w_0}{R_t} = N_{2\kappa}(\varphi) \quad (7)$$
$$\frac{1}{r}\cdot\frac{\partial u_0}{\partial \varphi} + \frac{\partial v_0}{\partial s} - \frac{v_0}{r} cos\ \theta = N_{3\kappa}(\varphi)$$

Here, (k = 0,1,2...) for k = 0:

$$N_{10}(\varphi) = \left(T_m - \frac{1}{2}T_t\right)/Eh;$$
$$N_{20}(\varphi) = \left(T_t - \frac{1}{2}T_m\right)/Eh; \quad (8)$$
$$N_{30}(\varphi) = 3S\ /\ Eh,$$

for k = 1:

$$N_{11}(\varphi)=\frac{1}{\varepsilon_0^2}\left(\frac{\partial u_0}{\partial s}+\frac{w_0}{R_m}\right)^3;$$

$$N_{21}(\varphi)=\frac{1}{\varepsilon_0^2}\left(\frac{1}{r}\cdot\frac{\partial v_0}{\partial\varphi}+\frac{u_0}{r}cos\ \theta+\frac{w_0}{R_t}\right)^3; \quad (9)$$

$$N_{31}(\varphi)=\frac{1}{\gamma_0^2}\left(\frac{1}{r}\cdot\frac{\partial u_0}{\partial\varphi}+\frac{\partial v_0}{\partial s}-\frac{v_0}{r}cos\ \theta\right)^3$$

for k = 2:

$$N_{12}(\varphi)=\frac{3}{\varepsilon_0^2}\left(\frac{\partial u_0}{\partial s}+\frac{w_0}{R_m}\right)^2\left(\frac{\partial u_1}{\partial s}+\frac{w_1}{R_m}\right);$$

$$N_{32}(\varphi)=\frac{3}{\gamma_0^2}\left(\frac{1}{r}\cdot\frac{\partial u_0}{\partial\varphi}+\frac{\partial v_0}{\partial s}-\frac{v_{10}}{r}cos\ \theta\right)^2 \quad (10)$$

$$\left(\frac{1}{r}\cdot\frac{\partial u_1}{\partial\varphi}+\frac{\partial v_1}{\partial s}-\frac{w_1}{r}cos\,\theta\right);$$

4.5. Numerical solution

We multiply both sides of **Equations 8** and **9** by ν and ν^2, respectively, and combine them with the corresponding **Equation 7**. Considering the third-order approximation for u, v, and w, the following system of linear equations is obtained:

$$\frac{\partial u}{\partial s}+\frac{w}{R_m}=N_{10}(\varphi)+\frac{\nu}{\varepsilon_0^2}N_{10}^3(\varphi)+\frac{3\nu^2}{\varepsilon_0^4}N_{10}^5(\varphi);$$

$$\frac{1}{r}\cdot\frac{\partial v}{\partial\varphi}+\frac{v}{r}cos\ \theta+\frac{w}{R_t}=N_{20}(\varphi)+\frac{\nu}{\varepsilon_0^2}N_{20}^3(\varphi)+\frac{3\nu^2}{\varepsilon_0^4}N_{20}^5(\varphi); \quad (11)$$

$$\frac{1}{r}\cdot\frac{\partial u}{\partial\varphi}+\frac{\partial v}{\partial s}-\frac{v}{r}cos\ \theta=N_{30}(\varphi)+\frac{\nu}{\gamma_0^2}N_{30}^3(\varphi)+\frac{3\nu^2}{\gamma_0^4}N_{30}^5(\varphi);$$

By eliminating the displacement components u and w, the system is reduced to a single differential equation for the circumferential displacement component v:

$$r\frac{\partial^2 v}{\partial s^2}-\frac{\partial}{\partial\varphi}\left(\frac{v}{R_m}\right)+\frac{v}{R_m}sin\ \theta=\frac{\partial}{\partial s}\left[rN_3(\varphi,s)-\frac{\partial N_1(\varphi,s)}{\partial\varphi}\right] \quad (12)$$

Here,

$$N_1(\varphi,s)=\frac{T_m-\frac{1}{2}T_t}{Eh}+\frac{\nu}{\varepsilon_0^2}\left(\frac{T_m-\frac{1}{2}T_t}{Eh}\right)^3+\frac{3\nu^2}{\varepsilon_0^4}\left(\frac{T_m-\frac{1}{2}T_t}{Eh}\right)^5$$

$$N_3(\varphi,s)=\frac{3S}{Eh}+\frac{\nu}{\gamma_0^2}\left(\frac{3S}{Eh}\right)^2+\frac{3\nu^2}{\gamma_0^4}\left(\frac{3S}{Eh}\right)^5 \quad (13)$$

4.6. Model verification and validation

The validity of the proposed nonlinear formulation was verified by considering the limiting case of linear elastic behavior. When the small parameter ν approaches zero, the nonlinear terms in the constitutive relations vanish, and the developed formulation reduces to the classical linear shell theory.

The results obtained for this limiting case were compared with the corresponding solutions of the classical linear formulation. A good agreement between the two approaches was observed, confirming the consistency of the proposed mathematical model and the correctness of the nonlinear formulation.

This verification demonstrates that the developed method provides the classical linear solution as a special case and can therefore be applied for further analysis of nonlinear stress–strain behavior of shell structures.

5. Experimental investigation of rotating-frame rollers

5.1. Experimental setup and test specimens

The nonlinear shell analysis presented in the previous section and the experimental investigation conducted in this section represent two complementary aspects of the offshore support-block launching process. The nonlinear analysis enables the evaluation of the stress–strain state of the pontoon structure under the considered loading conditions, its structural optimization, and the justification of its load-carrying capacity. However, the overall reliability of the technological process is determined not only by the strength of the pontoon structure. During the safe transportation and launching of the support block, the load is transferred through the rotating frame, where the rollers act as the primary load-bearing elements. Therefore, ensuring the reliable operation of the rotating frame requires an assessment of the capability of the rollers to safely withstand the applied loads. For this purpose, the load-carrying capacity improvement of the existing roller structures by filling their internal volume with composite material was experimentally investigated.

At the Heydar Aliyev Baku Deepwater Jackets Factory, a special rotating frame is used during the launching of offshore platform jacket support blocks into the sea. The movement of

the support blocks is ensured by rollers operating on the cylindrical upper surface of the rotating frame. Since different jacket support blocks have different masses, it became necessary to assess the load-carrying capacity of the rollers.

For this purpose, an experimental investigation was conducted. The main objective of the study was to determine the maximum load that the rollers used in the rotating frame could withstand. A total of eight roller specimens were tested, including four hollow rollers and four filled rollers. The experimental results were used to evaluate the load-carrying capacity and operational reliability of the rollers.

During the tests, eight roller specimens with an outer diameter of 168 mm, a wall thickness of 8 mm, and a length of 820 mm were investigated. Four of the specimens were hollow, while the remaining four were of a filled design. The main characteristics of the specimens are presented in **Table 1**.

Here, D denotes the outer diameter, t the wall thickness, and L the roller length.

The roller is a steel pipe section closed at both ends with 10 mm-thick metal plates, whose main function is to ensure the displacement of the support block sliding on the frame without being subjected to crushing.

The filled rollers were manufactured by filling the internal volume of hollow roller specimens with a composite material. The average density of the mixture is 2,670 kg/m^3. The main structural and physical characteristics of the rollers are presented in **Table 1**.

During the experiments, the loading conditions were adjusted to simulate real operating conditions. The stress–strain state was investigated under transverse static loading applied along the generator direction of the roller specimens.

The tests were carried out using a PSU-250 hydraulic press. Deformations in the cross-section of the specimens and changes in the vertical diametral direction were measured using indicators. The displacements were measured using indicators positioned along the horizontal and vertical diameters of the roller specimens. Filled rollers are used in rotating frames applied during the launching of support blocks of platform structures into the sea at the Heydar Aliyev Baku Deepwater Jackets Factory.

5.2. Experimental procedure

The specimens were subjected to transverse static loading using a hydraulic press. The deformation of the roller cross-section was measured by indicators installed along the horizontal and vertical diameters. Electrical strain gauges were used to determine the stress state during loading.

5.3. Material characterization

Prior to testing the roller specimens, standard material samples were tested to determine the stress–strain characteristics. The obtained results were used to define the yield strength of the steel material.

At the same time, electrical strain gauges with a 20 mm gauge length were used to determine the stress state of the specimens.

In the initial stage, standard material specimens were tested, and the results are presented in **Table 2**.

The experimental results showed that up to a stress level of 235 MPa, residual deformation remained after unloading. However, no yielding was observed at 235 MPa. Therefore, the yield strength of the material was taken as 235 MPa.

Subsequently, both hollow and composite-filled roller specimens were tested, and the results are presented in **Table 3**.

5.4. Load-carrying capacity results

The load–deformation behavior of hollow and composite-filled roller specimens under hydraulic compression is presented in the graphical abstract. The experimental results demonstrate

Table 1. Details of test specimens

Specimen nos.	Dimensions, mm (D × t × L)	Number of specimens	Type
1–4	168 × 8 × 820	4	Hollow
5–8	168 × 8 × 820	4	Filled with composite material

Table 2. Experimental results of material specimens

Load, kN	**Average strain gauge reading, Ω**	**Stress, MPa**
10	159	42.6
20	213	79.4
30	304.5	113.4
40	437	163.0
45	518	193.2
50	591	220.0
51	594	221.5
52	600	223.5
53	606	226.0
54	610	227.5
55	612	228.0
56	616	229.7
57	626	233.4
58	643	239.8
59	730	272.3
60	758	282.7
62	884	329.7
64	1,206	449.8
118	Failure	

Table 3. Experimental results of hollow and composite-filled cylindrical specimens

Specimen no.	Type of structure	Dimensions, mm	Maximum test load, kN	Horizontal diameter, mm	Vertical diameter, mm	Maximum test load per meter length, kN/m
1	Hollow	168 × 8 × 440	178	169.62	165.325	–
2	Hollow	168 × 8 × 440	173.4	169.28	166.111	–
3	Hollow	168 × 8 × 440	168.5	169.364	165.869	–
4	Hollow	168 × 8 × 440	177.3	169.329	165.973	–
Mean (hollow)			174.3	169.398	165.820	396.1
5	Composite-filled	168 × 8 × 440	364	169.040	166.079	–
6	Composite-filled	168 × 8 × 440	386	169.205	165.73	–
7	Composite-filled	168 × 8 × 440	439.5	168.081	165.67	–
8	Composite-filled	168 × 8 × 440	420	169.350	165.24	–
Mean (composite-filled)			402.4	169.919	165.680	914.5

that filling the internal volume of the rollers with composite material increased the maximum test load by approximately 2.3 times.

5.5. Statistical evaluation of experimental results

The statistical analysis confirms the repeatability of the experimental measurements (**Table 4**). Hollow specimens exhibited a coefficient of variation of 2.5%, indicating relatively stable behavior. The composite-filled specimens showed a higher variation (coefficient of variation = 8.4%), which can be attributed to variations in the distribution of the filling material and the interaction between the steel tube and composite core.

The deformation of the roller diameter is expressed as follows:

$$\Delta_x = \Delta_2 + \Delta_4,\ \Delta_y = \Delta_1 + \Delta_3 \tag{14}$$

where Δ_x and Δ_y represent the horizontal and vertical diametral deformations of the roller, respectively. Δ_i (i = 1 – 4) corresponds to the readings of indicators I1, I2, I3, and I4 (**Table A1**).

6. Results and discussion

Three nonlinear computational approaches were investigated and compared with the classical linear model. The obtained results show reductions in the maximum stress level of 10.3%, 7.3%, and 4.3% for the first, second, and third nonlinear approaches, respectively, compared with the linear formulation.

The comparison between linear and nonlinear formulations demonstrated a difference in the predicted stress values. The nonlinear model resulted in a 13.8% lower stress value compared with the linear approximation. The comparison of stress variations between the linear and nonlinear formulations is presented in **Figure 8**.

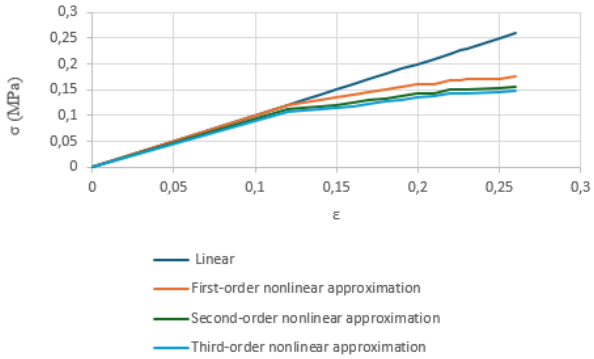


Figure 8. Comparison of the stress–strain responses predicted by the linear model and the first-, second-, and third-order nonlinear approximations

The lower stress levels predicted by the nonlinear formulation can be attributed to the redistribution of membrane forces within the shell structure. In linear analysis, material stiffness is assumed to remain constant, which may result in an overestimation of local stress concentrations. As illustrated in **Figure 8**, the nonlinear formulation provides a more realistic stress prediction compared with the linear model due to the redistribution of internal forces and the consideration of the nonlinear stress–strain relationship.

The influence of geometric modifications on the structural response was also evaluated. A reduction of 7.5% in the maximum stress level was obtained after modifying the geometric parameters of the structure. The analysis of geometric effects confirms that the structural response of thin-walled offshore components strongly depends on shell configuration. Therefore, accurate representation of the shell middle-surface geometry is essential for reliable strength assessment and structural optimization.

The convergence and accuracy of the proposed numerical approach were evaluated through verification cases. The calculated results showed stable convergence and good agreement with the reference linear solution for the limiting case when the nonlinear parameter approaches zero.

Table 4. Statistical analysis of experimental results

Type of Structure	Number of specimens (n)	Mean maximum test load, kN	Standard deviation, kN	Coefficient of variation, %	Lowest recorded test load, kN
Hollow	4	174.3	4.4	2.5	168.5
Composite-filled	4	402.4	33.8	8.4	364.0

The proposed methodology is particularly relevant for offshore launching systems, where pontoon structures are subjected to combined gravitational loads, buoyancy forces, and operational constraints. The interaction between the pontoon structure and supporting mechanisms influences the load transfer path and should be considered when evaluating overall structural reliability.

The comparison between nonlinear and classical linear approaches confirms that neglecting physical nonlinearity may lead to inaccurate estimation of structural safety margins. Therefore, the developed framework provides an effective tool for the analysis and optimization of offshore and hydraulic engineering structures subjected to complex loading conditions.

The experimental investigation of rotating-frame rollers demonstrated that the average maximum test load increased from 174.3 kN for hollow rollers to 402.4 kN for composite-filled rollers. Thus, the introduction of composite filling resulted in an approximately 2.3-fold increase in the measured load-carrying capacity of the roller specimens.

The substantial increase in the maximum test load of composite-filled rollers can be attributed to the interaction between the steel shell and the internal composite core. The filling material reduces local deformation of the thin-walled steel tube and improves the load transfer mechanism, resulting in enhanced resistance under transverse loading conditions. The increase in the maximum test load was achieved without modifying the external dimensions, material, or arrangement of the rollers, but only by introducing composite filling into the internal volume. This demonstrates the effectiveness of the proposed structural modification.

7. Conclusion and future research

The results of this study demonstrate that the application of nonlinear analysis methods improves the accuracy of stress–strain assessment of offshore and hydraulic engineering structures. The developed methodology considers material nonlinearity, geometric variability, and both symmetric and asymmetric loading conditions.

The proposed computational approach enables the analysis of thin-walled shell structures with circular cross-sections and variable thicknesses subjected to combined internal and external loads using the small parameter method. The developed formulation provides an effective tool for evaluating structural response and optimizing geometric parameters.

The nonlinear formulation was applied to the analysis of pontoon-type offshore structures used during launching operations. The obtained results demonstrate that consideration of nonlinear effects leads to stress redistribution and provides a more realistic estimation of the structural response compared with the classical linear approach.

The validity of the proposed formulation was confirmed by considering the limiting linear case. When the small parameter v approaches zero, the nonlinear model converges to the classical linear shell solution. The comparison between linear and nonlinear formulations demonstrates stress reductions of up to 13.8%, highlighting the importance of considering material nonlinearity in offshore structural analysis.

The proposed methodology provides a computational framework for investigating the strength and post-critical behavior of shells of revolution made of nonlinear elastic materials under complex loading conditions.

The experimental results confirmed that filling the hollow rollers with composite material significantly improves their structural performance. The average maximum test load increased from 174.3 kN to 402.4 kN, providing approximately a 2.3-fold improvement without changing the external dimensions or basic configuration of the rollers.

Despite the promising results, the present study has several limitations. The proposed model is developed for thin shells of revolution and considers quasi-static loading conditions. Dynamic effects, fatigue degradation, corrosion processes, and fluid–structure interaction are not included in the current formulation. Furthermore, the material behavior is described using a physically nonlinear elastic model, while time-dependent effects such as plasticity and damage accumulation require further investigation.

Future research will focus on extending the proposed framework to more complex engineering scenarios, including fluid–structure interaction, three-dimensional structural configurations, and time-dependent material behavior. Additional developments will include adaptive numerical procedures and optimization-based design strategies to improve computational efficiency and structural performance.

Acknowledgments

None.

Funding

None.

Conflict of interest

The authors declare they have no competing interests.

Author contributions

Conceptualization: All authors
Methodology: All authors
Investigation: All authors
Writing–original draft: Latif F. Aslanov, Firidun L. Aslanov
Writing–review & editing: Ulvi L. Aslanli, Firidun L. Aslanov

Availability of data

The data supporting the findings of this study are available from the corresponding author upon reasonable request. The experimental data and calculated results presented in this article can be provided to interested readers upon request.

AI tools statement

All authors confirm that no AI tools were used in the preparation of this manuscript.

References

1. Al-Mubarak, A., Younus, Y.M. Study the effect of blast load on the steel offshore platforms. *Asian J Civ Eng.* 2025;26:1847-1864.

   https://doi.org/10.1007/s42107-025-01290-2

2. Amaechi CV, Reda A, Butler HO, Ja'E IA, An C. Review on fixed and floating offshore structures. Part I: Types of platforms with some applications. *J Mar Sci Eng.* 2022;10(8):1074.

   https://doi.org/10.3390/jmse10081074

3. Bhardwaj, U., Teixeira, A.P. & Guedes Soares, C. Probabilistic Risk model of Ship Allision Accidents with Offshore Platforms. J. Marine. *Sci Appl.* 2026;25:713-727.

   https://doi.org/10.1007/s11804-026-00812-1

4. Chalkina, A.A., Lobanov, A.V. Second Life of Offshore Oil and Gas Platforms. *Power Technol Eng.* 2025;58:563-570.

   https://doi.org/10.1007/s10749-025-01849-8

5. Cheng X, Jia C, Luo B. Reduced sloshing effect in steel tanks. *Int J Steel Struct.* 2022;22:1474-1496.

   https://doi.org/10.1007/s13296-022-00652-9

6. ElHamahmy, A. Overview of shock absorbers for boat landings on fixed offshore platforms. *Mar Syst Ocean Technol.* 2026;21:3.

   https://doi.org/10.1007/s40868-025-00198-5

7. Filippenko GV. The vibrations of reservoirs and cylindrical supports of hydro technical constructions partially submerged into the liquid. In: Evgrafov A, ed. *Advances in Mechanical Engineering. Lecture Notes in Mechanical Engineering.* Cham, Switzerlaand: Springer; 2016:115-126.

   https://doi.org/10.1007/978-3-319-29579-4_12

8. Gurkalo F, He C, Poutos K, He N. Effects of innovative reinforced concrete slit shaft configuration on seismic performance of elevated water tanks. *Sci Rep.* 2024;14:6113.

   https://doi.org/10.1038/s41598-024-56851-3

9. Holtschoppen B, Knoedel P. Seismic response of slender storage tanks on tube feet or skirt support. *Bull Earthquake Eng.* 2024;22:55-73.

   https://doi.org/10.1007/s10518-023-01704-z

10. Huseynli, A., *Öztürk*, S., Erkmen, B. et al. Seismic Response Assessment of Topside Equipment on Fixed Offshore Platforms. *Iran J Sci Technol Trans Civ Eng.* 2026;50:2817-2834.

    https://doi.org/10.1007/s40996-025-01951-x

11. Iskandarov EKh. Study of structural changes in multifaceted gas pipelines. *SOCAR Proc.* 2024;(4):117-122.

    https://doi.org/10.5510/OGP20240401026

12. Iskandarov EKh, Ismayilova FB, Shukurlu MF, Ismayilova PSh. Changes in energy characteristics of pipeline systems considering hydrodynamic loads. *SOCAR Proc.* 2024;(2):105-108.

    https://doi.org/10.5510/OGP20240200974

13. Kovtun AV, Tabunenko VO, Nesterenko S, et al. Determining the strength of tanks with fluid in the case of free dropping. *Int Appl Mech.* 2023;59:107-113.

    https://doi.org/10.1007/s10778-023-01204-2

14. Kumaravel, T., Wijewardhana, A.S. & Ratnayake, A.S. Lifecycle structural integrity assessment of single point anchor reservoir (SPAR) offshore platforms using a composite degradation index. *Mar Syst Ocean Technol.* 2026;21(3):32.

    https://doi.org/10.1007/s40868-026-00230-2

15. Agapov VP, Vasil'ev A. Account for geometrical nonlinearity in the analysis of reinforced concrete columns of rectangular section by finite element method. *Vestn MGSU*. 2014;(4):37-43. https://cyberleninka.ru/article/n/uchet-geometricheskoy-nelineynosti-pri-raschete-zhelezobetonnyh-kolonn-pryamougolnogo-secheniya-metodom-konechnyh-elementov

16. Aslanov LF, Aslanli UL. Investigation of the elastic-plastic behavior of pipes and vertical risers in offshore hydraulic structures. *Int J Optim Control Theor Appl*. 2026;16(3):1064-1085.

https://doi.org/10.36922/IJOCTA026090035

17. Aydin AC, Yaman Z, Ağcakoca E, Kiliç M, Maali M, Aghazadeh Dizaji A. CFRP effect on the buckling behavior of dented cylindrical shells. *Int J Steel Struct*. 2020;20(2):425-435.

https://doi.org/10.1007/s13296-019-00294-4

18. Bathe KJ, Brezzi F, Marini LD. The MITC9 shell element in plate bending: mathematical analysis of a simplified case. *Comput Mech*. 2011;47:617-626.

https://doi.org/10.1007/s00466-010-0565-2.

19. Borwein J, Skerritt M. *An Introduction to Modern Mathematical Computing: With Mathematica*. New York, NY: Springer; 2012.

https://doi.org/10.1007/978-1-4614-4253-0

20. Bovo M, Barbaresi A, Torreggiani D. Definition of seismic performances and fragility curves of unanchored cylindrical steel legged tanks used in wine making and storage. *Bull Earthq Eng*. 2020;18(8):3711-3745.

https://doi.org/10.1007/s10518-020-00841-z

21. Chapelle D, Bathe KJ. *The Finite Element Analysis of Shells: Fundamentals*. Berlin, Germany: Springer; 2003.

https://doi.org/10.1007/978-3-662-05229-7

22. Chikhi, A., Djermane, M. Effect of local geometrical imperfection on dynamic buckling of cylindrical storage tanks. *Asian J Civ Eng*. 2018;19:189-203.

https://doi.org/10.1007/s42107-018-0017-4

23. Eliseev, V.V., Vetyukov, Y.M. Finite deformation of thin shells in the context of analytical mechanics of material surfaces. *Acta Mech*. 2010:209:43-57.

https://doi.org/10.1007/s00707-009-0154-7

24. Gadjiyev MA, Guseynov IG, Gadjiyeva UM. Stress-strain state and load ability of compressed pipe-concrete elements. *SOCAR Proceedings*. 2023;(Special Issue No.1):21-26.

https://doi.org/10.5510/OGP2023SI100836.

25. Giampieri A, Perego U. An interface finite element for the simulation of localized membrane-bending deformation in shells. Comput Methods *Appl Mech Eng*. 2011;200(29-32):2378-2396.

https://doi.org/10.1016/j.cma.2011.04.009

26. Hansen ELMB, Silva FMA. Nonlinear vibration analysis of a partially filled multi-layer cylindrical tank: consideration of the sloshing effects in the fluid–structure interaction. *J Braz Soc Mech Sci Eng*. 2022;44:484.

https://doi.org/10.1007/s40430-022-03800-8

27. Mansouri I, Farzampour A. Buckling assessment of imperfect cylindrical shells under axial loads using a GEP technique. *Adv Civ Archit Eng*. 2018;9(17):89-100.

https://doi.org/10.13167/2018.17.9

28. Kılıç M. Buckling behavior of nose cone type steel tanks including horizontal imperfection. *Int J Steel Struct*. 2021;21(4):1408-1419.

https://doi.org/10.1007/s13296-021-00512-y

29. Labiodh B, Chalane M. Effect of localized defect positioning on buckling of axisymmetric cylindrical shells under axial compression. *Mech Solids*. 2023;58:880-889.

https://doi.org/10.3103/S0025654423600046

30. Lebedev AE, Kapranova AB, Gudanov IS, Dolgin DS, Vatagin AA. Study of the influence of annular plate size on the stress-strain state of a vertical steel tank. *Chem Pet Eng*. 2021;57:239-245.

https://doi.org/10.1007/s10556-021-00924-x

31. Li Y, Fu J, Qian L, Wang HY. On the discussions of nonlinear terms in the large deformation model of thin-walled cylindrical shells. *Mech Solids*. 2023;58:1214-1227.

https://doi.org/10.3103/S0025654423600216

32. Gulin M, Uzelac I, Dolejš J, Boko I. Design of liquid-storage tank: results of software modeling vs calculations according to Eurocode. Elektronički *časopis* građevinskog fakulteta Osijek. 2017;8(15):85-97.

https://doi.org/10.13167/2017.15.8

33. Santos PR, Donadon MV. A semi-analytical model for buckling and stress analyses of pressurized composite cylinders. *J Braz Soc Mech Sci Eng*. 2023;45:484.

https://doi.org/10.1007/s40430-023-04350-3

34. Sholomitskii AA, Tsarenko SN, Mogilny SG, Aukazhieva ZM, Kemerbaev NT. Evaluation of stress-strain state of vertical steel tanks using laser scanning data. In: Radionov AA, Gasiyarov VR, eds. *Proceedings of the 8th International Conference on Industrial Engineering (ICIE 2022)*. Lecture Notes in Mechanical Engineering.

Heidelberg, Germany: Springer; 2023:881-890.

https://doi.org/10.1007/978-3-031-14125-6_86

35. Milić P, Marinković D, *Ćojbašić* Ž. Geometrically nonlinear analysis of piezoelectric active laminated shells by means of isogeometric FE formulation. *Facta Univ Ser Mech Eng.* 2025;23(2):387-405.

https://doi.org/10.22190/FUME050123059M

36. Sun Y, Wang C, Wang W, Li T, Yang T. Dynamic response analysis of a small-scaled ACLNG storage tank under penetration and explosion loadings. *Acta Mech Sin.* 2023;39:123110.

https://doi.org/10.1007/s10409-023-23110-x

37. Wang W, Mottershead JE, Sebastian CM, Patterson EA. Shape features and finite element model updating from full-field strain data. *Int J Solids Struct.* 2011;48(11-12):1644-1657.

https://doi.org/10.1016/j.ijsolstr.2011.02.010

38. Yang L, Zhang S, Qiu T. Buckling analyses of cylindrical shells with axial variable elastic modulus under external pressure. *J Braz Soc Mech Sci Eng.* 2024;46:163.

https://doi.org/10.1007/s40430-024-04742-z

39. Zhang H, El Ansary AM, Zhou W. Nonlinear buckling analysis of conical steel tanks considering field-measured imperfections—a case study. In: Walbridge S, Nik-Bakht M, Ng KTW, et al., eds. *Proceedings of the Canadian Society of Civil Engineering Annual Conference 2021: CSCE21 General Track Volume 2.* Lecture Notes in Civil Engineering. Vol 240. Heidelberg, Germany: Springer; 2023:295-306.

https://doi.org/10.1007/978-981-19-0507-0_28

40. Zinovieva T. Calculation of shells of revolution with arbitrary meridian oscillations. In: Evgrafov A, ed. *Advances in Mechanical Engineering. Lecture Notes in Mechanical Engineering.* Heidelberg, Germany: Springer; 2017:165-176.

https://doi.org/10.1007/978-3-319-53363-6_17

41. Aslanov LF, Aslanli UL. Study of the stress-strain state of the pontoon element of the support block. *SOCAR Proc.* 2024;(2):115-121.

https://doi.org/10.5510/OGP20240200976.

42. Aslanov LF, Aslanli UL, Aslanov FL. New calculation method for the pontoon element of offshore fixed platforms for oil and gas production. *Nafta-Gaz.* 2025;(3):188-198.

https://doi.org/10.18668/NG.2025.03.05

Latif F. Aslanov *has over 30 years of academic and engineering experience in the field of marine hydrotechnical structures, offshore oil and gas platforms, and the strength, stability, and reliability of their foundations and structural systems. He worked at SOCAR's Oil-Gas Research and Design Institute, where he held positions including Research Associate, Leading Research Associate, Head of the Laboratory of Marine Hydrotechnical Structures, and Head of the Technical Production Department. He is currently an Associate Professor at Azerbaijan University of Architecture and Construction. His research interests include the bearing capacity of pile foundations, pile–soil interaction, the strength and stability of offshore platform structural elements, their behavior under static, dynamic, and seismic loads, and the development of rational design and engineering calculation methods. He is the author and co-author of numerous scientific publications and normative and methodological documents.*
https://orcid.org/0000-0003-1546-5436

Ulvi L. Aslanli *is Chief Structural Engineer at SOCAR Downstream Management, where he is responsible for reviewing structural designs, engineering documentation, and multidisciplinary Engineering, Procurement, and Construction (EPC) projects in accordance with international engineering standards and project requirements. He is also a lecturer in the Department of Foundations and Underground Structures at Azerbaijan University of Architecture and Construction. He has more than nine years of academic and professional experience in structural and geotechnical engineering, with expertise in structural analysis, soil and foundation engineering, engineering software, project management, and risk management. He holds a Master's degree in Construction Engineering and Management and an MBA, and is currently pursuing a Ph.D. in Structural Engineering, focusing on the stress–strain behavior of marine hydraulic structures. He is also a certified PMP, PMI-ACP, PMI-RMP, and PMI-PBA, and has authored several peer-reviewed scientific publications.*
https://orcid.org/0009-0001-1504-5258

Firidun L. Aslanov *is currently working as a Specialist at SOCAR Türkiye and has nearly 10 years of professional experience at SOCAR. During his career, he has gained experience in the installation, dismantling, and operation of oil and gas facilities, as well as pipeline design, project budget planning, and management. He holds a Bachelor's and a Master's degree in Oil and Gas Facilities Engineering, as well as Master's degrees in Business Administration (General) and Business Administration (Finance). He has authored several peer-reviewed papers and works closely with industry professionals to connect theory and practice. He also holds PMP, PMI-ACP, PMI-PBA, FMVA, ACCA Diploma in Accounting and Business, and CIMA CertBA certifications.*
https://orcid.org/0009-0005-1039-0748

Appendix

Nomenclature (symbols and terminology)

As shown in **Table A1**, the symbols and terminology used in this analysis are defined systematically to enhance clarity and ensure consistency throughout the paper.

Table A1. Nomenclature of symbols used in the analysis

Symbol	Definition	Unit	Application/Comment
T_m	Meridional stress resultant	N/m	Normal force acting along the meridian direction
T_t	Tangential stress resultant	N/m	Normal force acting in the circumferential direction
S	Shear stress resultant	N/m	Shear force acting on shell cross-sections
P_1	Normal component of external distributed load	N/m^2	Loading on shell surface
P_2	Meridional component of external distributed load	N/m^2	In-plane directional load
P_3	Tangential component of external distributed load	N/m^2	Circumferential loading effect
R_m	Radius of curvature in meridional direction	m	Shell geometry parameter
R_t	Radius of curvature in circumferential direction	m	Shell geometry parameter
r	Radial coordinate	m	Current spatial coordinate
θ	Shell inclination angle	rad	Geometric parameter defining shell orientation
φ	Circumferential coordinate	rad	Angular coordinate
s	Meridional coordinate	m	Coordinate measured along the shell meridian
ε_m	Meridional normal strain	–	Deformation in meridional direction
ε_t	Circumferential (tangential) normal strain	–	Deformation in hoop direction
γ_{tm}	In-plane shear strain	–	Shear deformation in shell middle surface
u	Meridional displacement	m	Displacement component along the meridian
v	Tangential displacement	m	Displacement component along the circumferential direction
w	Normal displacement	m	Displacement component perpendicular to the shell surface
E	Elastic modulus	Pa	Material stiffness parameter in normal deformation
G	Shear modulus	Pa	Material stiffness parameter in shear deformation
h	Shell thickness	m	Geometric parameter of the shell structure

(*Cont'd...*)

Table A1. (*Continued*)

Symbol	Definition	Unit	Application/Comment
μ	Poisson's ratio	–	Ratio between transverse and longitudinal deformation
β	Nonlinear coefficient in normal stress–strain relation	Pa	Governs the cubic nonlinear term in normal stress response
β_0	Nonlinear coefficient in the shear stress–strain relationship	Pa	Governs the cubic nonlinear term in shear stress response
σ	Normal stress	Pa	Stress–strain constitutive relation variable
v	Small material nonlinearity parameter	–	Expansion parameter in asymptotic series solution
ε_0	Characteristic normal strain	–	Reference strain value used in the nonlinear constitutive relation
γ_0	Characteristic shear strain	rad	Reference shear strain value used in the nonlinear constitutive relation
u_j	(j)-th order meridional displacement coefficient	m	Coefficient of the power series expansion of displacement (u)
v_j	(j)-th order tangential displacement coefficient	m	Coefficient of the power series expansion of displacement (v)
ω_j	(j)-th order normal displacement coefficient	m	Coefficient of the power series expansion of displacement (w)
j	Expansion order index	–	Series expansion counter (j = 0,1,2,...)
u_0	Zero-order meridional displacement component	m	First approximation term of the meridional displacement series
v_0	Zero-order tangential displacement component	m	First approximation term of the tangential displacement series
w_0	Zero-order normal displacement component	m	First approximation term of the normal displacement series
N_{ik} (i = 1,2,3)	Components of internal force resultants at order k	N/m	Terms in recursive differential system
k	Perturbation/recursion order index	–	Series expansion level (k=0,1,2,...)
$N_{1к}(\varphi)$	Nonlinear strain function in the meridional direction	Dimensionless	Represents nonlinear contribution to the meridional deformation equation
$N_{2к}(\varphi)$	Nonlinear strain function in the circumferential direction	Dimensionless	Represents nonlinear contribution to the circumferential deformation equation
$N_{3к}(\varphi)$	Nonlinear shear strain function	Dimensionless	Represents nonlinear contribution to the shear deformation equation
$N_{10}(\varphi)$	Zero-order meridional function	Dimensionless	Right-hand-side function of the zero-order meridional equation
$N_{20}(\varphi)$	Zero-order tangential function	Dimensionless	Right-hand-side function of the zero-order tangential equation
$N_{30}(\varphi)$	Zero-order shear function	Dimensionless	Right-hand-side function of the zero-order shear equation
$N_{11}(\varphi)$	First-order meridional nonlinear function	Dimensionless	Cubic nonlinear term associated with the meridional strain

(*Cont'd...*)

Table A1. (*Continued*)

Symbol	Definition	Unit	Application/Comment
$N_{21}(\varphi)$	First-order tangential nonlinear function	Dimensionless	Cubic nonlinear term associated with the tangential strain
$N_{31}(\varphi)$	First-order shear nonlinear function	Dimensionless	Cubic nonlinear term associated with the shear strain
$N_{12}(\varphi)$	Second-order meridional nonlinear function	Dimensionless	Second-order contribution of the meridional strain to the recurrent system
$N_{22}(\varphi)$	Second-order tangential nonlinear function	Dimensionless	Second-order contribution of the tangential strain to the recurrent system
$N_{32}(\varphi)$	Second-order shear nonlinear function	Dimensionless	Second-order contribution of the shear strain to the recurrent system
$N_1(\varphi,s)$	Meridional nonlinear function	Dimensionless	Function appearing in the reduced governing equation
$N_3(\varphi,s)$	Shear nonlinear function	Dimensionless	Function representing the shear contribution in the reduced equation
Δx	Horizontal diametral deformation of the roller	m	Total horizontal deformation obtained from the indicator readings
Δy	Vertical diametral deformation of the roller	m	Total vertical deformation obtained from the indicator readings
Δ_i	Indicator displacement reading (i=1,2,3,4)	m	Measured displacement recorded by the corresponding indicator
I_1,I_2,I_3,I_4	Displacement indicators	Dimensionless	Instruments used to measure the roller deformation



This work is licensed under a Creative Commons Attribution 4.0 International License. The authors retain ownership of the copyright for their article, but they allow anyone to download, reuse, reprint, modify, distribute, and/or copy articles in IJOCTA, so long as the original authors and source are credited. To see the complete license contents, please visit http://creativecommons.org/licenses/by/4.0/.